North Atlantic Interannual Variability in a Coupled Ocean–Atmosphere Model

THOMAS L. DELWORTH

Geophysical Fluid Dynamics Laboratory/NOAA, Princeton, New Jersey

(Manuscript received 25 May 1995, in final form 14 December 1995)

ABSTRACT

The primary mode of sea surface temperature variability in the North Atlantic on interannual timescales during winter is examined in a coupled ocean–atmosphere model. The model, developed at the Geophysical Fluid Dynamics Laboratory, is global in domain with realistic geography and a seasonal cycle of insolation. Analyses performed on a 1000-year integration of this model show that this mode is characterized by zonal bands of SST anomalies in the North Atlantic and bears a distinct resemblance to observational results. The largest anomalies in the model are to the southeast of Newfoundland.

The model SST variations appear to be related to a north–south dipole in the atmospheric 500-mb geopotential height field, which resembles the North Atlantic oscillation and the Western Atlantic pattern. Analyses are presented that show that this mode of SST variability is primarily driven by perturbations to the surface heat fluxes, which are largely governed by atmospheric variability. Changes in model ocean circulation also contribute to this mode of variability but appear to be of secondary importance.

Additional integrations are analyzed to examine the above conclusion. The same atmospheric model used in the above integration was coupled to a 50-m slab ocean and integrated for 500 years. The primary mode of SST variability in this model, in which there were no effects of ocean dynamics, resembles the primary mode from the coupled model, strengthening the conclusion that the surface fluxes are the primary mechanism generating this oceanic variability. One notable difference between the two models is related to the presence of deep vertical mixing at high latitudes in the model with a fully dynamic ocean. An additional 500-year integration of the atmospheric model with a prescribed seasonal cycle of SSTs lends further support to this conclusion, as do additional diagnostic calculations in which a 50-m slab ocean was forced by the time series of surface fluxes from both the prescribed SST and fully coupled model.

1. Introduction

One of the key goals of climate research is to obtain a better understanding of climate and its variability on seasonal to interdecadal timescales. This goal demands an improved understanding of interactions between the ocean and the atmosphere, which constitute one of the key links in the climate system. An important paradigm for interpreting these interactions was offered by Bjerknes (1964), who hypothesized that sea surface temperature variations in the North Atlantic on interannual timescales are primarily forced by atmospheric variability, whereas SST variations on much longer timescales (decadal and longer) are a manifestation of internal oceanic variability.

This paper focuses on interannual timescale variability of SSTs in the North Atlantic of a coupled ocean–atmosphere model. Specifically, the following questions are asked: 1) How well does a coupled model of the ocean–atmosphere system simulate the observed SST variability in the North Atlantic region on *interannual* timescales? 2) What are the mechanisms by which that model variability is generated?

A number of observational studies have characterized North Atlantic interannual variability. Most of these studies have focused on the Northern Hemisphere winter season, thereby motivating us to also concentrate on that season in this paper. Bjerknes (1964) demonstrated that there are distinct modes of SST variability on interannual and interdecadal timescales. The interannual mode is characterized by alternating zonal bands of SST anomalies. Wallace and Jiang (1987) and Wallace et al. (1990) have documented the fundamental modes of variability in the atmosphere–ocean system over the North Atlantic during the winter season. They find, in agreement with Bjerknes (1964), that the primary mode of SST variability over the North Atlantic is characterized by zonal bands of SST anomalies. Furthermore, this mode is associated with changes in atmospheric circulation over the North Atlantic region (as will be shown in section 3a). Zorita et al. (1992) have also found that the dominant modes of SST variability in the North Atlantic during winter are associated with clear signatures of atmospheric variability. They conclude that "These results are consistent with the hypothesis that anomalies of the atmospheric circulation are mainly responsible for the appearance of

Corresponding author address: Dr. Thomas L. Delworth, GFDL/NOAA, P.O. Box 308, Princeton, NJ 08542.
E-mail: td@gfdl.gov

anomalous wintertime SST . . .". Kushnir (1994) has also examined variability in the North Atlantic and finds similar structures of SST and atmospheric variability. Cayan (1992a,b) has demonstrated that variations in the surface latent and sensible heat fluxes over the North Atlantic appear to drive this primary mode of interannual SST variability.

Relationships have also been ascertained between SST anomalies on decadal timescales and atmospheric variability. Deser and Blackmon (1993) have examined low frequency (decadal and longer) oceanic and atmospheric variability over the North Atlantic. In addition to a multidecadal trend in SSTs, they find a mode of variability on the decadal timescale. This mode is characterized by anomalies of one sign east of Newfoundland and anomalies of opposite sign off the southeast United States. This mode is strongly related to atmospheric circulation anomalies, as well as to decadal variations of sea ice. Recently, Halliwell (1996, manuscript submitted to *J. Climate*) has found a clear association between oceanic and atmospheric variability in the North Atlantic on decadal and longer timescales.

Modeling studies have also addressed the issue of how interannual SST variability in the North Atlantic is generated. Daly (1978) examined the roles of both oceanic advection and surface heat flux variations in generating SST anomalies. Frankignoul (1985) showed that a substantial portion of oceanic variability may be viewed as the response of the oceanic mixed layer to stochastic atmospheric forcing. Battisti et al. (1995) have demonstrated that SST variations in the North Atlantic may be explained largely through surface heat flux variations. Alexander and Deser (1995) have demonstrated how midlatitude SST anomalies may persist from one winter to the next.

A number of modeling studies have explored the impact that SST anomalies in the North Atlantic have on atmospheric circulation. Palmer and Sun (1985) examined the response of an atmospheric model to prescribed SST anomalies in the northwest Atlantic. Their results, supported by Ferranti et al. (1994), suggest that such SST anomalies may alter the atmospheric circulation over the North Atlantic and Europe. Lau and Nath (1990) examined the response of an atmospheric GCM to the prescription of observed SST anomalies for the period 1950–79. Their results suggest a connection between atmospheric variability over the North Atlantic and SST fluctuations. Peng et al. (1995) have shown that the atmospheric response to SST anomalies may be highly dependent on the mean climatological state. In their study, the response in November to an SST anomaly is quite different from the response in January to the same prescribed SST anomaly.

Much of the previous modeling work has focused on ocean-only models or atmospheric models with either prescribed SSTs or coupled to a mixed layer of the upper ocean. It is desirable to examine North Atlantic SST variability within the context of a fully coupled ocean–atmosphere model. Such a model should contain a rich spectrum of air–sea interactions. A number of multicentury integrations with a coupled ocean–atmosphere model have recently been conducted at the Geophysical Fluid Dynamics Laboratory (Stouffer et al. 1994; Manabe and Stouffer 1996). Such extended integrations provide an important opportunity to compare model variability to observations. The output from one of these integrations forms the basis for many of the analyses described in this paper. The variability simulated in this model is due solely to internal variability of the *coupled* ocean–atmosphere system and thus provides an ideal setting for diagnosing the role of air–sea interactions in generating North Atlantic SST variability.

The focus of the present paper is on the interannual variability in the North Atlantic of this coupled model. It should be noted that the model variability to be examined is distinctly different from that shown in Delworth et al. (1993), who describe a 40–60 year timescale variation in the intensity of the thermohaline circulation (THC) in the North Atlantic of this coupled model. As described later, temporal filtering is performed to effectively remove the THC multidecadal signal from the model output.

The outline of this paper is as follows: In section 2 a brief description is presented of the coupled ocean–atmosphere model, the design of the integration, and the model's climatology over the North Atlantic region. In section 3 the variability in the model ocean and atmosphere is described and compared to observed variability. The mechanism of the model variability as inferred from heat budget diagnostics is presented in section 4, and results from additional integrations of the atmospheric model with either a mixed layer ocean or prescribed SSTs are shown in section 5. A summary and discussion is presented in section 6.

2. Model description

a. Model description

The model used in this study consists of an atmospheric general circulation model (AGCM) coupled to an oceanic general circulation model (OGCM). The AGCM is formulated from the primitive equations and solves the equations numerically using a spectral technique (Gordon and Stern 1982). The model resolution is rhomboidal 15, corresponding approximately to a horizontal resolution of 7.5° longitude and 4.5° latitude. There are nine unevenly spaced layers in the vertical. There is a seasonal cycle of insolation but no diurnal cycle. Clouds are predicted whenever the relative humidity exceeds a critical value (99%) [moist convective adjustment is used—see Manabe et al. (1965).] A constant mixing ratio of carbon dioxide and a zonally uniform, seasonally varying value of ozone are prescribed.

The basic structure of the oceanic component of the model is similar to the model described by Bryan and Lewis (1979). The finite difference mesh used for the time integration of the primitive equations of motion has a spacing between grid points of 4.5° latitude and 3.75° longitude. It has 12 unevenly spaced levels for finite differencing in the vertical direction. Spacing of the levels increases with depth: the top layer has a thickness of 50.9 m, while the bottom layer has a thickness of 868 m. The model uses realistic bottom topography (smoothed to model resolution) with a maximum depth of 5000 m. The model predicts sea ice using a simple model developed by Bryan (1969). One difference from the model used in Bryan and Lewis (1979) is that the present model has isopycnal mixing, as discussed by Tziperman and Bryan (1993), in addition to horizontal and vertical background subgrid-scale mixing and convective overturning.

The coupled model is global in domain, with realistic geography consistent with the resolution. The atmospheric and oceanic components interact with each other through the exchanges of heat, water (including ice), and momentum at their interface. The water/ice flux includes runoff from the continents to the oceans. For further details of the model formulation, see Manabe et al. (1991, 1992). The model integrations analyzed in this study are the same as those conducted and described by Stouffer et al. (1994) and Manabe and Stouffer (1996).

b. *Time integration*

When the time integration of a model starts from an initial condition that is not in equilibrium, the model climate usually undergoes a drift toward an equilibrium state. Such a drift contaminates the natural variability of the model climate, which is the subject of the present study. Thus, it is highly desirable that the initial condition for the time integration be as close to equilibrium as possible.

Manabe and Stouffer (1988) have shown that a time integration of the original version of their model yielded an unrealistic equilibrium state, characterized by an exaggerated halocline in high latitudes and the absence of a significant thermohaline circulation in the North Atlantic. To offset this bias of the model, they adjusted the flux of water at the oceanic surface by an amount that varies geographically and seasonally but does not change from one year to the next during the integration of the model. In the present study, this adjustment is performed for the fluxes of both water and heat at the oceanic surface. The seasonal and geographical distributions of the adjustment have no interannual variations. In addition, since the flux adjustments are computed prior to the integration of the coupled model, the adjustments do not depend in any way on the magnitude of the SST or sea surface salinity anomalies. Thus, the adjustments do not explicitly affect the feedback processes that reduce these anomalies and neither amplify nor dampen anomalies of SST or sea surface salinity. The adjustments also ensure that fluctuations of the model climate are around a realistic mean. This can be a critical issue, since the mechanisms and nature of variability can be dependent upon the mean state. The specific details on the determination of the initial quasi-equilibrium condition and the flux adjustment are described by Manabe et al. (1991, §3b).

Starting from an initial condition in quasi-equilibrium, the coupled model is time-integrated over a period of 1000 years. The mean rate of change in global mean sea surface temperature of the model over this period is very small (~0.02°C/century).

c. *Model climatology in the North Atlantic region*

Before examining the variability results in the next section, it is desirable to document the model climatology in the winter season, which is the focus of this paper. Shown in Fig. 1 are the long-term mean SST and 500-mb geopotential height fields for December through February (DJF) averages for both model and observations. The model climatologies are computed over all 1000 years of the integration. The SST climatology, obtained from the U.K. Meteorological Office (Bottomley et al. 1990) on a 5° latitude–longitude grid, is based on an average over the period 1951–1980. The observed 500-mb height field is the DJF mean over the period 1946–1992. The data were obtained from the U.S. National Meteorological Center on a 5° longitude by 2.5° latitude grid north of 20°N.

The simulated SST field corresponds closely to the observed field (note that the flux adjustments are designed to accomplish this). There are no contours for the observations in Baffin Bay or the northwest part of the Greenland Sea due to both the presence of sea ice and lack of observations.

The 500-mb height field generally resembles observations, although model heights are lower than observed values, reflecting a cold bias of the model. In both the model and observations the axis of a major trough extends from the Arctic southward over Baffin Bay and Hudson Bay. Another major trough in both the model and observations is located along the eastern edge of the Asian continent. The flow over the Atlantic (inferred geostrophically from the height field) is generally similar in the model and observations, with a weak ridge over western Europe.

The simulated currents in the North Atlantic (see Fig. 1 of Delworth et al. 1993) resemble observations in pattern, although substantially weaker in magnitude. There is a distinct Gulf Stream and North Atlantic Current, as well as both the subtropical and subpolar gyre. The relative weakness of the currents may be related

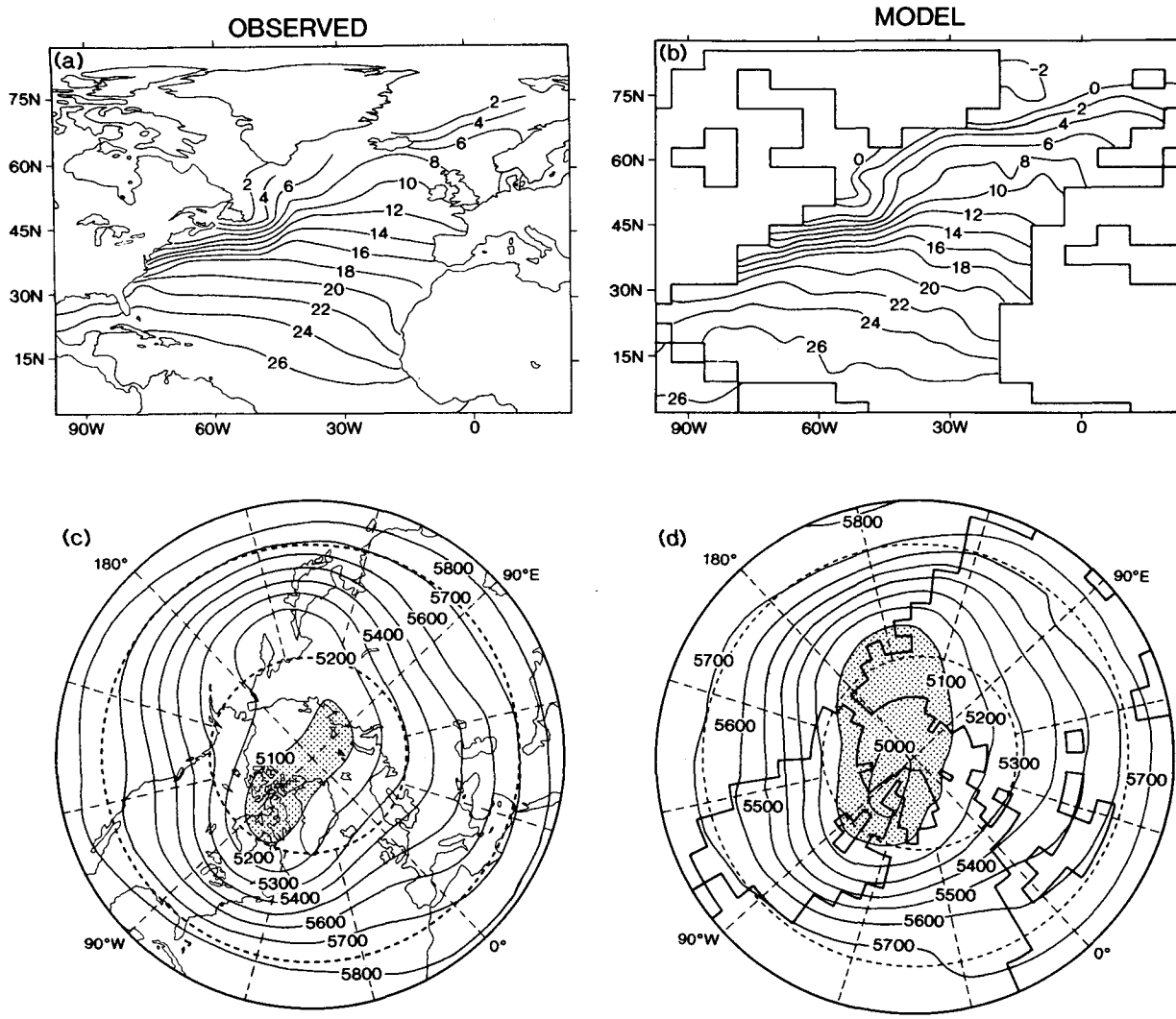

FIG. 1. Long-term mean SST field over the North Atlantic for DJF (a) from observations over the period 1951–80 and (b) for the model output. Units are degrees Celsius. Long-term mean 500-mb geopotential height field for DJF (c) from observations over the period 1946–92 and (d) for the model output. Units are geopotential meters. Values less than 5100 are stippled.

both to the coarse resolution of the model and to the presence of model diffusion.

3. North Atlantic variability results

a. Oceanic variability

Wallace et al. (1990) used an empirical orthogonal function analysis to characterize the primary mode of SST variability in the North Atlantic for DJF [for a discussion of EOF analysis, see Kutzbach (1967) or Preisendorfer (1988)]. Their analysis employed a 39-year period from 1946 to 1984, and the results of their analysis for the Atlantic poleward of 20°N are shown in Fig. 2a. The contoured field denotes the correlation coefficients at each grid point between the time series corresponding to the EOF pattern and the time series of SST at that grid point. This mode of variability (explaining 24% of the spatially integrated variance) consists of alternating zonal bands of positive and negative SST anomalies. The largest correlation coefficients are in the western part of the basin.

Previous analyses (Delworth et al. 1993) of the output from the coupled model used in this study have shown that the dominant mode of oceanic variability in the North Atlantic is a fluctuation of the thermohaline circulation, with a timescale of approximately 40–60 years. An EOF analysis of the model SST data with no temporal filtering yields a first EOF (not shown) related to this very low frequency oceanic mode. In order to better study the shorter timescales, the model SST data was filtered such that fluctuations with timescales longer than 30 years were effectively removed.

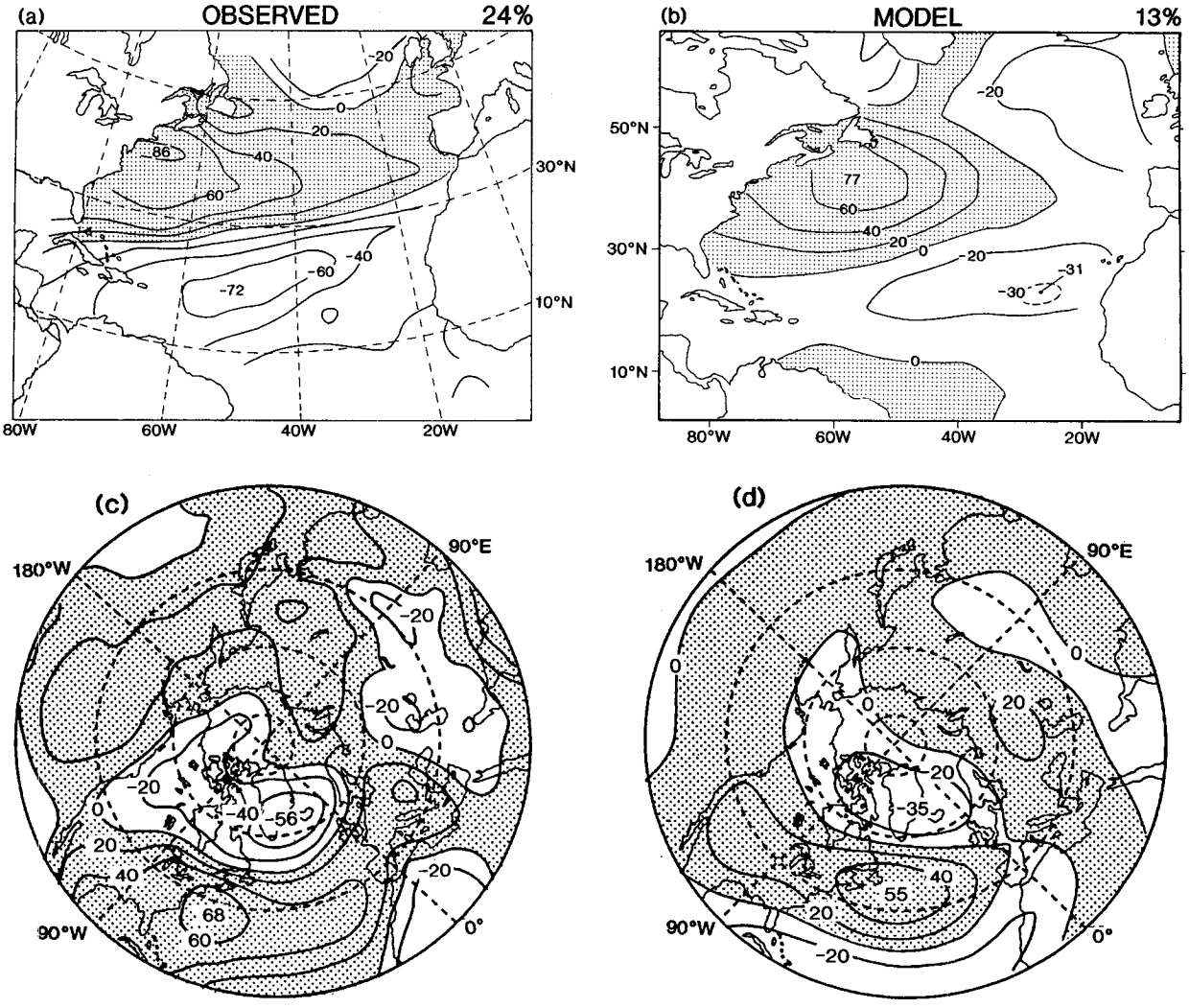

FIG. 2. (a) Spatial pattern of the first EOF of seasonal mean (Dec–Feb) observed SST (redrafted from Wallace et al. 1990) explaining 24% of the spatially integrated variance. The value at each grid point denotes the correlation coefficient (multiplied by 100) between the time series of the first EOF and the time series of observed SST at that point. The EOF analysis used the covariance matrix and encompassed a domain in the North Atlantic north of 20°N. Values greater than zero are stippled. (b) Spatial pattern of the first EOF of seasonal mean (Dec–Feb) model SST, explaining 13% of the spatially integrated variance. The value at each grid point denotes the correlation coefficient (multiplied by 100) between the time series of the first EOF and the time series of model SST at that point. The EOF analysis used the covariance matrix and encompassed a domain extending from approximately 18° to 63°N in the North Atlantic. Prior to the EOF analysis, the model SST data were filtered such that timescales longer than 30 years were removed from the data. In addition, SST values were multiplied by the square root of the cosine of the latitude in order to weight the grid boxes by their respective area. Values greater than zero are stippled. Shown in (c) and (d) are the correlation coefficients (multiplied by 100) between the time series of 500-mb geopotential heights and the first EOF of SST from (c) observations (redrafted from Wallace et al. 1990) and (d) model data. The contour interval is 20. Values greater than zero are stippled.

The filter employed the finite impulse response method with 200 weights (Bloomfield 1976, pp. 129–137). While the length of the model integration was 1000 years, only years 101–900 of the filtered dataset were employed in the subsequent analyses in order to avoid any possible contamination by the filter due to the finite length of the time series. The details of the filtering are not important to the results of the analyses below; it was only essential to remove the low-frequency variations.

An EOF analysis was then performed on the 800-year time series of filtered model SST data over the North Atlantic from 18° to 63°N. Time means for December through February were used. It should be noted that what is referred to in this study as model "SST" is actually the temperature of the top 50.9-m layer of the model ocean. The results, shown in Fig. 2b, reveal some degree of resemblance between the model and observational results. (Note that realistic geography is used in this figure to facilitate comparison of the model

and observed results. Subsequent figures dealing with model analyses use model geography.) Both patterns are zonally oriented in nature, with the largest correlation coefficients in the western part of the basin near the northeastern United States and maritime provinces of Canada. In terms of magnitude, the maximum model SST anomalies associated with this EOF pattern are approximately 0.5° to 1°C off the northeastern U.S. coast. This is slightly less than observational results [see Fig. 11a of Kushnir (1994)]. The model pattern, however, does not extend as coherently across the North Atlantic at around 40°N as the observational results do. Between 15°N and 30°N, the model correlation coefficients are larger in the eastern part of the basin, whereas the observational correlation coefficients are larger in the central part of the basin. These differences between the model output and observations highlight the need for model improvements to attain a more realistic simulation. Nevertheless, we feel that the first EOF of model SST variability resembles the observational results.

It should be noted that while the observational analyses are based on a 39-year dataset, the model analyses utilize 800 years of data. Additional EOF analyses were performed on nine nonoverlapping 39-year subsets of the model data. While there are some variations of the dominant EOF pattern between the subsets, most bear a substantial resemblance to that seen in Fig. 2b. In addition, the percentage of variance explained by these EOFs computed from the shorter time series ranged from 14% to 21%. Therefore, the smaller fraction of variance seen in Fig. 2b (compared to Fig. 2a) may be partially attributable to the larger sample size used for Fig. 2b.

b. Atmospheric variability

In order to assess the associations (if any) between this mode of oceanic variability and the overlying atmosphere, linear correlations were computed between the time series of the EOFs and the time series of 500-mb geopotential height anomalies at each grid point. The results from observations (Wallace et al. 1990) are shown in Fig. 2c, and the corresponding model results are shown in Fig. 2d. For both the model and observations, the first EOF of SST is associated with a north–south dipole in 500-mb height, with resemblance to both the North Atlantic oscillation (NAO) and the Western Atlantic pattern (see, for example, Walker and Bliss 1932; van Loon and Rogers 1978; Wallace and Gutzler 1981). A stronger than normal Icelandic low (as indicated by the negative correlation values over southeastern Greenland) and a stronger than normal subtropical high (indicated by the positive values in the subtropics of the North Atlantic) are associated with the SST anomaly pattern indicated in Figs. 2a and 2b. Analyses in section 4a using surface pressure will demonstrate that the model atmospheric variability described above is equivalent barotropic. It will be shown in the next section that the model SST anomaly patterns may be interpreted as the oceanic response to variations in the intensity of the atmospheric circulation in the North Atlantic, and hence the surface heat fluxes, corresponding approximately to the NAO variations.

A singular value decomposition (SVD) analysis was conducted using the model SST and 500-mb height fields and yielded results similar to Fig. 2 [see Bretherton et al. (1992) for a discussion of the SVD technique). The first SVD pair (not shown) explained 58.4% of the squared covariance. Further, the data used as input for this SVD analysis were the unfiltered time series of SST and 500-mb height (although linear trends were removed from the time series at each grid point prior to analysis). Thus, while EOF analysis of unfiltered model SST reveals a mode related to the multidecadal THC variations previously described (Delworth et al. 1993), SVD analysis of unfiltered SST and 500-mb height shows that the mode in Fig. 2 explains the largest fraction of the covariance between the model SST and 500-mb height.

There are notable differences, however, between the model and observed atmospheric 500-mb-height patterns. In the observations the correlations are positive from approximately 50°N to at least as far south as 20°N. In the model results the correlations are positive from approximately 55°N to 30°N, but are negative south of 30°N. In addition, the maximum positive correlation in the observations is off the northeastern United States, while the maximum in the model is off the Newfoundland coast.

In order to determine whether the pattern of 500-mb height anomalies shown in Fig. 2d represents a fundamental mode of model atmospheric variability, an EOF analysis was performed on model 500-mb height anomalies poleward of 20°N (the time series of 500-mb height anomalies was not subjected to any filtering other than removing the seasonal cycle from the raw 500-mb height data; the only dataset in this study that was filtered was the time series of SST). This analysis used DJF means, and the EOFs were rotated using the varimax technique [see Horel (1981) for a discussion of varimax rotation—this technique is designed to emphasize regional patterns]. The first EOF of model 500-mb height anomalies is shown in Fig. 3. This mode, explaining 13.4% of the spatially integrated variance, is similar over the North Atlantic region to the pattern shown in Fig. 2d (note that the sign convention is arbitrary). This suggests that the atmospheric variability associated with the primary mode of model SST variability in the North Atlantic is itself a fundamental mode of atmospheric variability in the model. One difference between the two is that between 30°N and 50°N the pattern in the Atlantic extends farther toward Europe in Fig. 3 than in Fig. 2d.

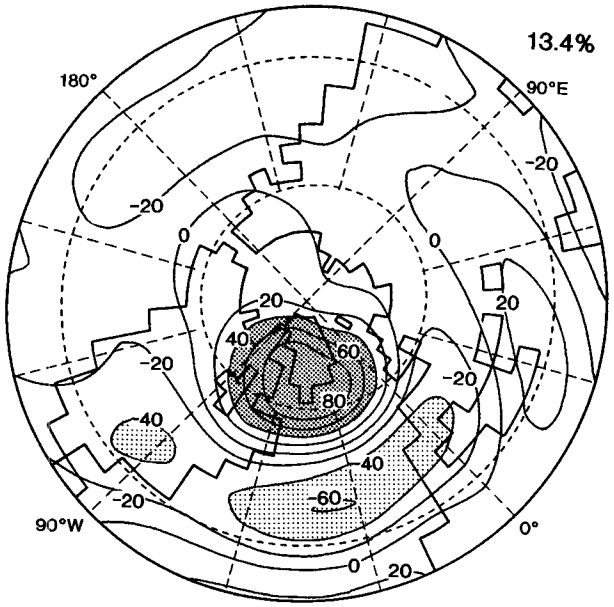

FIG. 3. Spatial pattern of the first EOF computed from model 500-mb geopotential height anomalies averaged over the Dec–Feb season (a varimax rotation was performed). This mode explains 13.4% of the spatially integrated variance. The domain of analysis consisted of all points north of 20°N. The values contoured represent the correlation coefficients (multiplied by 100) between the time series of 500-mb geopotential height anomalies at each grid point and the EOF time series. Contour interval is 20. Values less than −40 are lightly stippled, and values greater than +40 are densely stippled.

To characterize the temporal scale of this atmospheric variability, the spectrum of the time series associated with the EOF in Fig. 3 is shown in Fig. 4a. Note that the spectrum is fairly flat, with no enhancement of variance at low frequencies (in fact, the largest spectral estimates occur at relatively high frequencies). This may be contrasted with the spectrum of the time series associated with the first EOF of model SST, shown in Fig. 4b. (The time series for SST EOF 1 is computed by projecting the spatial pattern of the EOF mode onto the unfiltered SST. In this manner, there are variations in the EOF time series at timescales longer than 30 years.) This spectrum is "red," with greater variance at low frequencies than at high frequencies. This increase of variance at low frequencies is consistent with the stochastic theory of climate variability as discussed by Hasselmann (1976). In this theory, climate variability can be generated as the red noise response of a system to white noise forcing (the system behaves as a first-order Markov process). For the particular case of SST variability, the time series of surface heat flux variations (which has spectral characteristics similar to white noise) drives the oceanic mixed layer. The thermal inertia of the mixed layer results in slowly varying SST anomalies in response to the white noise surface flux forcing. It will be shown later that the spatial pattern of the surface flux forcing is similar to the pattern of the model SST anomalies.

4. Mechanisms of variability

Our focus in this paper is on the mode of SST variability shown in Fig. 2b (and Fig. 2a for the observational results). While it has been shown that the model variability resembles that observed in nature, we would also like to examine the mechanisms by which that model variability is generated.

The SST variability can be generated in several ways: 1) atmospheric variability forcing oceanic variability, 2) internal oceanic variability, relatively independent of the atmosphere, or 3) coupled air–sea interactions. In this section we shall provide analyses that seek to explore the roles of these processes.

a. Temporal relationship between oceanic SST anomalies and atmospheric circulation

In order to assess whether the oceanic variability is being forced from the atmosphere or generated via in-

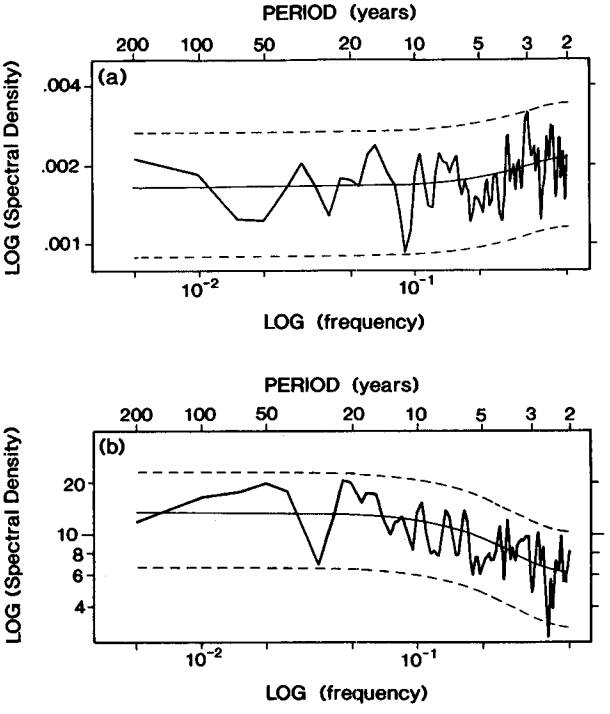

FIG. 4. (a) Spectrum of the time series associated with the EOF pattern in Fig. 3 for model 500-mb height anomalies. Periods in years are listed along the top. The spectrum was computed by taking the Fourier transform of the autocovariance function, using a maximum of 100 lags and a Tukey window (Chatfield 1989, chapter 7). The thick, solid line denotes the spectral estimates. The thin, solid line denotes a red noise spectrum (corresponding to a first-order Markov process) with the same lag one autocorrelation as the original time series. The dashed lines represent the 95% confidence limits about the red noise spectrum. (b) Same as (a) but for the time series associated with the EOF pattern in Fig. 2b for model SST.

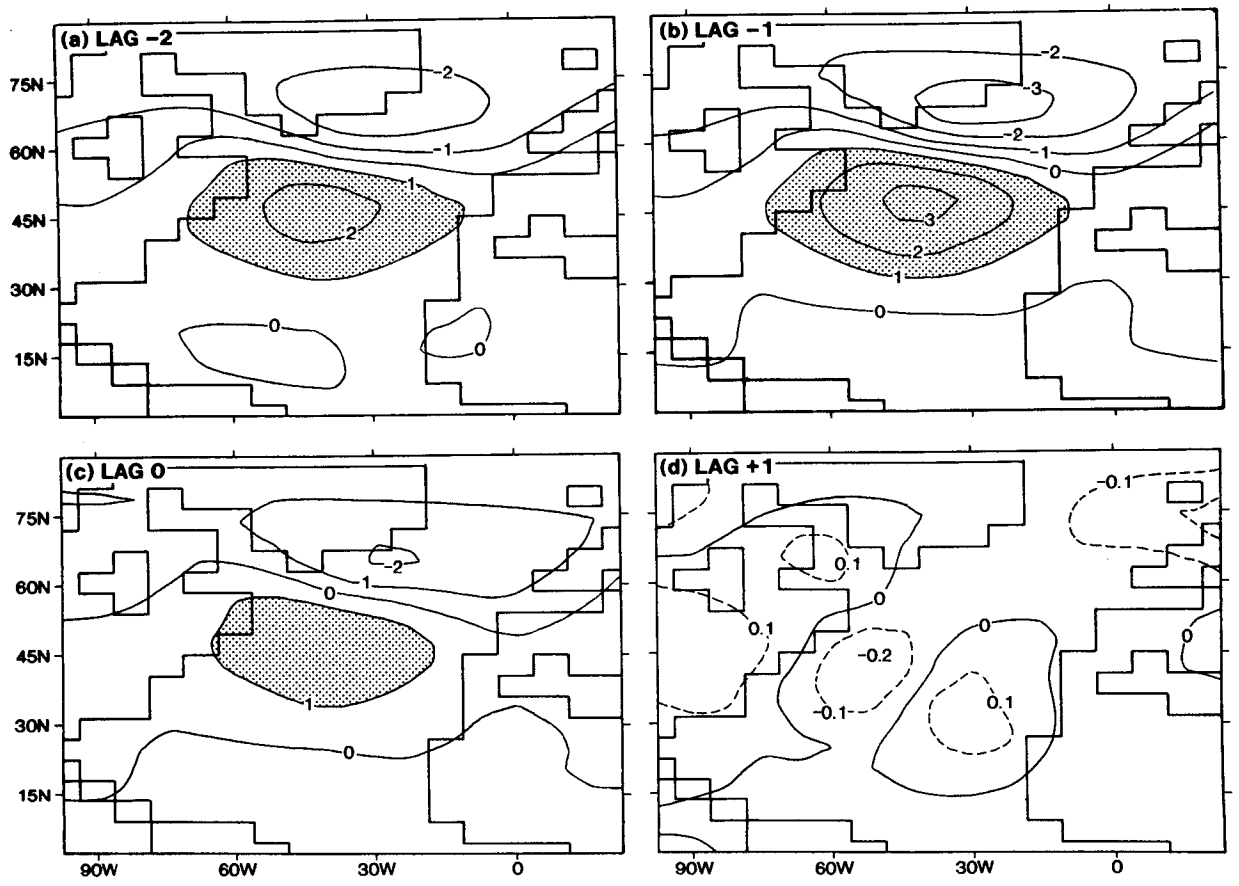

FIG. 5. Lagged regressions between the time series of surface pressure and the EOF coefficient time series for SST. Regressions are computed using data from November through March. A lag of −1 (+1) indicates conditions 1 month prior (subsequent) to a maximum in the SST pattern indicated in Fig. 2b. Units are mb. Contour interval is 1, and values greater than +1 are stippled. (a) Lag −2 months, (b) lag −1 months, (c) lag 0 months, and (d) lag +1 months.

ternal oceanic processes, it is useful to compute lagged regressions between surface pressure at each grid point and the time series associated with the EOF pattern of SST. Such analyses will indicate whether or not the atmospheric circulation anomalies associated with the SST pattern precede the SST anomaly, thereby indicating possible forcing of the ocean by the atmosphere [see, for example, Wallace and Jiang (1987) for an example of this type of analysis]. Surface pressure is used here instead of 500-mb height because of its more direct link with the oceanic state, but analyses with 500-mb height data yield results similar to those shown below.

The analyses up to this point have been restricted to data averaged over the months of December–February. In order to compute lagged regressions, EOFs of SST were computed using monthly data from November through March. The EOF analysis, therefore, used 4000 points in time (5 winter months for each of 800 years). The resultant pattern (not shown) was extremely similar to that shown in Fig. 2b. The domain for this analysis was extended to 81°N, but this had little influence on the results. The time series associated with this new EOF spatial pattern has values defined for the months of November through March for each of the 800 years and will be used for the regression analyses below.

Specifically, we will compute linear regressions of the form

$$y(t) = ax(t - \tau) + b, \qquad (1)$$

where $x(t)$ is the time series associated with the EOF pattern of SST, t is time, τ is the lag in months, a is the slope of the regression line and b its intercept, and $y(t)$ is the time series of surface pressure (or some other variable) at a grid point. These regressions are computed at each model grid point and provide an indication of how variables change in relation to the strength of the SST pattern. For example, regressions computed with lag (i.e., τ) equal to −1 (+1) denote surface pressure conditions 1 month prior (subsequent) to the SST conditions denoted by the spatial pattern in Fig. 2b. The field of values of a is contoured to provide an indication of the change in quantity y (surface pres-

sure, or some other field) for a unit change in x (the time series of the EOF coefficients).

Shown in Fig. 5 are contour maps of the slopes of the regression lines of surface pressure at each grid point versus the time series of the EOF coefficients for SST at lags −2, −1, 0, and +1 months. These regression coefficients (and all subsequent regression coefficients) have been multiplied by a factor of 3. This was done because the EOF coefficient time series has a standard deviation of 2.2. Since the regressions represent the change in surface pressure (mb) per unit change in the EOF coefficient time series, multiplying the regressions by a value somewhat larger than the standard deviation provides an indication of the magnitude of the surface pressure anomalies for relatively large excursions of SST. Specifically, 16.4% of the points in the EOF time series have absolute value greater than or equal to 3. As shown below, the surface pressure anomalies in Fig. 5 (maximum absolute values of approximately 3 mb) are associated with a maximum SST anomaly of 0.8°C off the coast of North America (the spatial pattern of which is indicated in Fig. 2b). Equivalently, a 1°C SST anomaly off North America would be associated with a 4-mb surface pressure anomaly.

It is clear from Fig. 5 that surface pressure leads the SST anomalies. Surface pressure anomalies, as indicated by the regression coefficients, have their largest magnitudes at lag −1 month. The asymmetry of the anomalous surface pressure about lag 0 (contrast lags −1 and +1) indicates that the anomalous surface pressure (atmospheric circulation) is leading the anomalous SST conditions. The conditions depicted for lag +1 are particularly striking: one month after the SST conditions are maximum there is virtually no anomaly in surface pressure, thereby suggesting that there is very little effect of the SST anomaly pattern on surface pressure *in this model.* The model conditions at lag −1 bear a resemblance to observational analyses (see Fig. 11b of Kushnir 1994). The anomalous circulation associated with the surface pressure anomalies indicates enhanced westerlies between approximately 50°N and 65°N.

Lagged *correlations* of surface pressure were also computed (not shown). The spatial patterns were very similar to those of the lagged regressions. The maximum positive correlation at lag −1 was 0.52 in the central North Atlantic, with a minimum correlation of −0.35 over extreme southeastern Greenland. Consistent with the regression analyses, correlations were essentially zero for lag +1 at all grid points (the maximum absolute value of any correlation was 0.05 at this lag).

In order to further characterize the oceanic variability, regressions were computed between the time series of SST at each grid point versus the time series of the EOF coefficients. The results, shown in Fig. 6, characterize the magnitude and temporal evolution of the SST anomaly pattern. The maximum SST anomalies, occurring at lag 0, are approximately 0.8°C off the eastern coast of North America. Note that unlike surface pressure, the SST anomalies persist past lag 0 due to the large thermal inertia of the model ocean.

The phase relationship shown in Fig. 5 demonstrated that atmospheric variability is leading the oceanic variability. We may infer from this (and subsequent analyses) that the atmospheric variability is *forcing* the oceanic variability. Such an influence can be achieved in at least two ways: 1) through the momentum forcing of the ocean by the anomalous atmospheric circulation, which thereby alters the oceanic circulation and the horizontal and vertical heat advection, and 2) through anomalous surface heat flux forcing of the upper ocean, thereby altering the heat content of the near-surface layer. Analyses in the next section will evaluate terms in the heat budget for the oceanic surface layer to quantify the importance of these processes in generating the SST anomalies shown in Fig. 2b and Fig. 6.

b. *Oceanic heat budget*

The heat budget for the uppermost oceanic layer in the model can be expressed by

$$C\frac{\partial T}{\partial t} = -C\mathbf{v}\cdot\nabla T - \mathrm{LH} - \mathrm{SH} + R + \mathrm{convt} - \mathrm{diffusion} + \mathrm{adjustment}. \quad (2)$$

In this equation, T is the temperature of the uppermost ocean layer, C is the heat capacity of the layer (mass of the layer times the specific heat), $\mathbf{v}$ is the three-dimensional velocity, ∇T is the three-dimensional gradient of temperature, LH is the latent heat flux, SH is the sensible heat flux, R is the net radiative forcing at the surface, "convt" is the equivalent heat flux corresponding to the temperature change due to oceanic convection, "diffusion" is the equivalent heat flux corresponding to the sum of horizontal and vertical diffusion, and "adjustment" represents the heating due to the flux adjustments (described in section 2b). All terms can be expressed as W m^{-2} for a 50.9-m layer. It should be stressed that, since the flux adjustments are precisely the same from one year to the next, there are no anomalies of this term. Therefore, flux adjustments make no direct contribution to this variability.

In a similar manner as for surface pressure and SST in the previous section, linear regressions were computed for various terms in (2) versus the time series of the EOF coefficients for SST. Shown in Fig. 7 are the regressions of the time derivative of SST[1] at each point.

[1] The time derivatives of SST for month n were estimated as one-half the SST at month $n + 1$ minus the SST at month $n - 1$. This is an approximation since the model SST values represent averages over an entire month. (The units are °C mo^{-1}.)

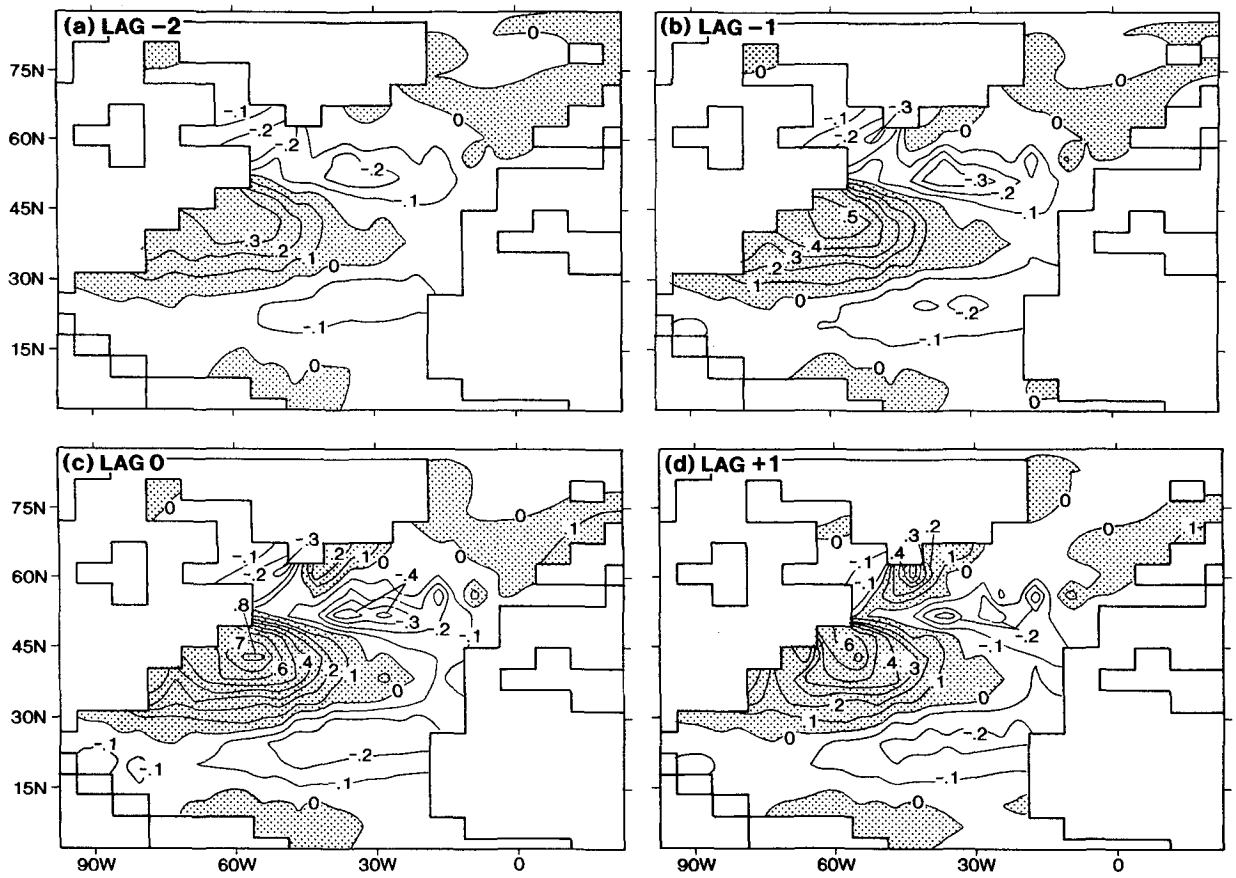

FIG. 6. Same as in Fig. 5 except using SST instead of surface pressure. Units are degrees Celsius. Contour interval is 0.1. Regions with values greater than zero are stippled.

The spatial pattern of the time derivatives of SST is consistent with the spatial pattern and temporal evolution of the SST anomalies in Fig. 6. Note that with the exception of the region off the southernmost tip of Greenland, the time derivatives generally have a minimum in absolute values at lag 0 and opposite signs for positive and negative lags.

In order to diagnose the processes responsible for the temporal changes in SST shown in Fig. 7, regressions were computed between various terms in the heat balance [right side of (2)] versus the time series of the EOF coefficients. Shown in Fig. 8 are the regressions for total heat advection (the sum of the zonal, meridional, and vertical components) in the uppermost ocean layer. In order to facilitate comparison with other terms in the heat balance, the advection terms (originally in units of °C s^{-1}) were converted to an equivalent surface heat flux for the 50.9-m uppermost model layer and expressed as W m^{-2}. Note that while oceanic heat advection was not routinely archived from the model output, monthly mean values of ocean temperature and velocity were used to estimate time series of heat advection for all 1000 years of the integration. These computations were performed using the same finite-difference operators as the model.

The spatial pattern of the oceanic heat advection anomalies for lags −2 and −1 is similar to that of the time derivatives of SST, thereby demonstrating that ocean advection contributes to the generation of the SST pattern in Figs. 2b and 6. Note that the pattern of anomalies is well organized for negative lags, but weakens for the lag 0 and lag +1 cases. It will be shown below that while anomalies of oceanic advection contribute to the spatial pattern of the SST anomalies in Figs. 2b and 6, the magnitude of the advection terms is less than the magnitude of the surface heat flux terms. The spatial pattern of advection anomalies is consistent with Ekman drift produced by the near-surface wind anomalies (inferred from Fig. 5) acting on the climatological gradient of SST (Fig. 1).

Shown in Fig. 9 are the lagged regressions of the sensible heat flux anomalies at the surface versus the time series of the EOF coefficient for SST. As was the case for surface pressure, the maximum surface flux anomalies occur before the maximum SST anomaly, again suggesting that atmospheric vari-

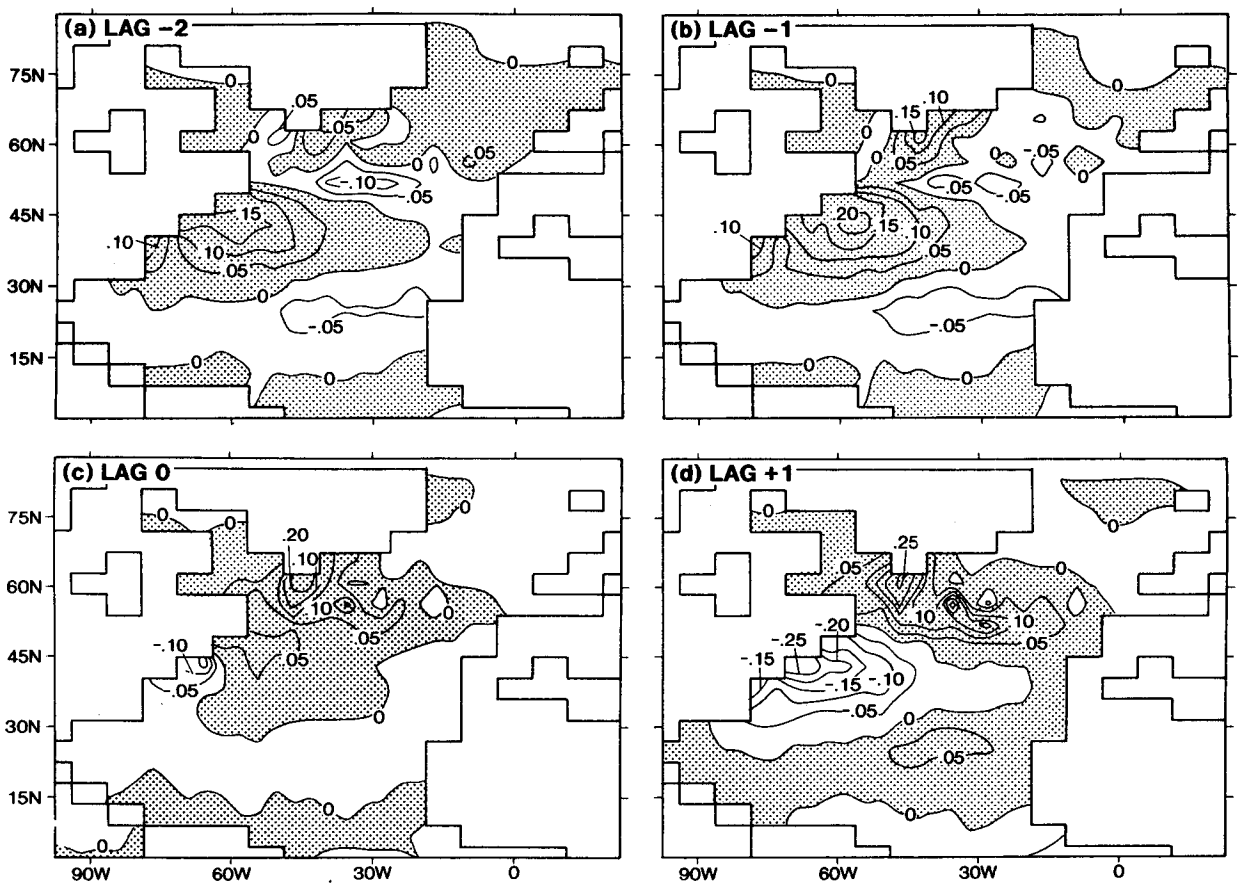

FIG. 7. Same as in Fig. 5 except using $\partial SST/\partial t$ instead of surface pressure. Units are degrees Celsius per month. Contour interval is 0.05. Regions with values greater than zero are stippled.

ability is driving the oceanic variability. An important point is that the surface flux anomalies represent both a forcing of the ocean by the atmosphere (due to anomalous wind speed, air temperature, and humidity) and a damping of SST anomalies. Anomalous SST perturbs the air–sea gradient of temperature and moisture, thereby influencing the surface heat fluxes in such a way as to damp the SST anomalies.

Shown in Fig. 10 are the lagged regressions for the latent heat flux anomalies, which have a pattern quite similar to the sensible heat flux anomalies. One small difference occurs near the northwest coast of Africa, where the latent heat anomalies are larger than the sensible heat anomalies. This is consistent with observational results (Cayan 1992a), where sensible heat flux anomalies are generally larger than latent heat flux anomalies at higher latitudes, whereas latent heat flux anomalies play a more prominent role in lower latitudes. This latitudinal gradient of the relative importance of the sensible and latent heat fluxes is largely a result of the dependence of the saturation vapor pressure of water on temperature.

Cayan has examined variations in observed surface heat flux anomalies for times with extreme values of the NAO. The patterns of model surface heat flux anomalies shown in Figs. 9 and 10 bear a distinct resemblance to the patterns derived from the observations (see Fig. 5 of Cayan 1992a). However, the model variations in the surface heat flux anomalies have a substantially smaller amplitude than the observed variations (on the order of one-half as large).

Combining the anomalous fluxes shown in Figs. 9 and 10 indicates a maximum total surface heat flux of approximately 20–25 W m^{-2}, although the total fluxes over most regions are smaller. For comparative purposes, 20 W m^{-2} acting on a layer of water 50.9 m thick (the thickness of the top layer of the ocean model) would produce a temperature change of 0.23°C mo^{-1}, consistent with the magnitude of the maximum rates of SST change associated with this EOF mode (see Fig. 7). This result suggests that the surface heat flux anomalies are able to quantitatively explain the magnitude of the SST anomalies. In addition, the magnitude of the total surface heat flux anomalies exceeds that from the oceanic heat advection anomalies, suggesting that the

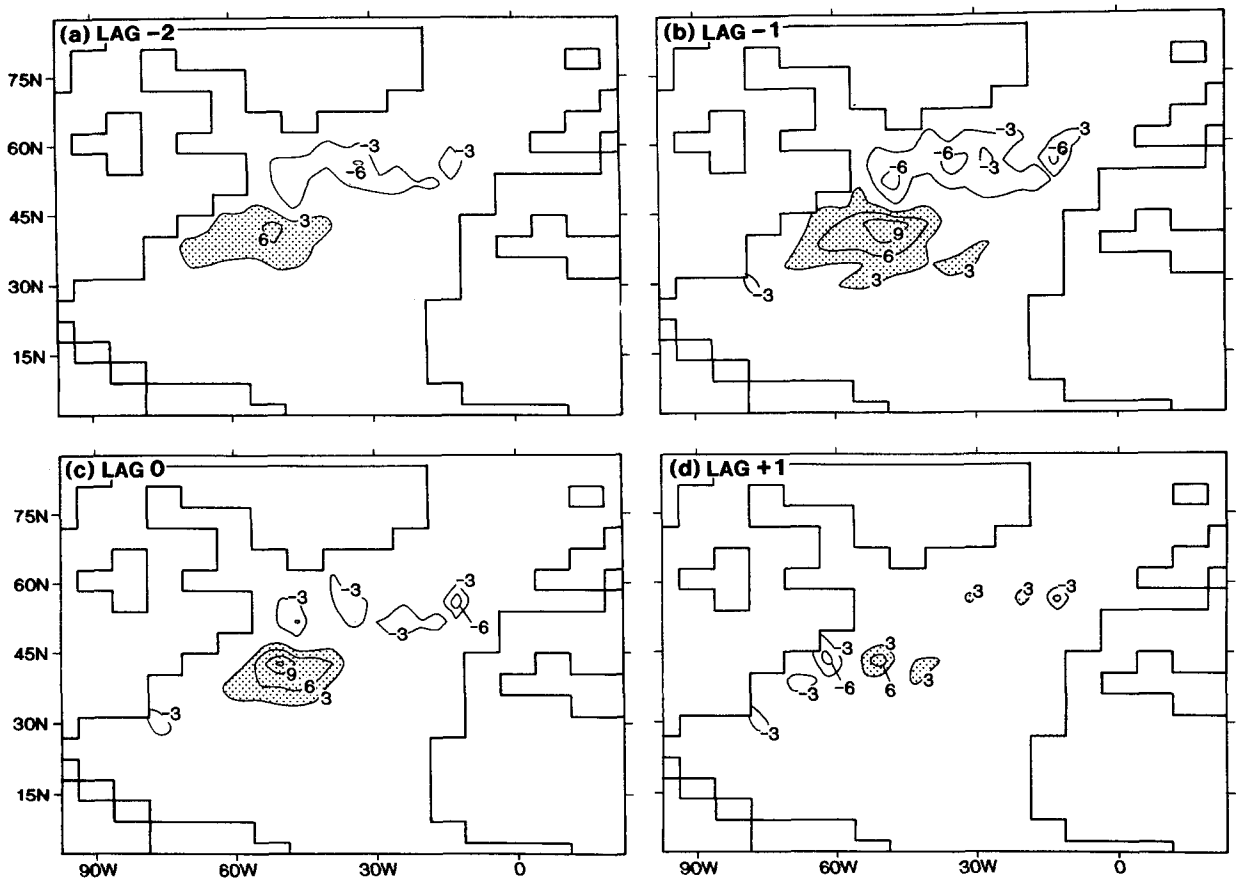

FIG. 8. Same as in Fig. 5 except using heat advection instead of surface pressure. The heat advection is then expressed as an equivalent surface heat flux for a 50.9-m layer. Units are watts per square meter. Contour interval is 3. Regions with values greater than 3 are stippled. Positive values indicate that anomalies of heat advection are acting to warm the surface layer.

former process plays a somewhat larger role than the latter.

Regressions of the effects of oceanic convection on SST (not shown) revealed that while this term is fairly small over most regions, it is large just to the south of Greenland. This term is responsible for the positive values of the time derivative of SST in that region (see Fig. 7) for lags −2 to +1. The anomalous surface heat fluxes perturb the stability of the water column, thereby altering the rates of convection. The region just to the south of Greenland is one of the principal areas for oceanic convection in the model.

Regressions were also computed between the anomalous surface radiative fluxes (difference between incoming shortwave and outgoing longwave) and the time series corresponding to the first EOF of SST. The regression coefficients (not shown) were small (maximum absolute values of approximately 3 W m^{-2}), suggesting that anomalies in the surface radiative forcing play only a minor role in this mode of SST variability. Diffusive terms were not available for evaluation.

In summary, these analyses demonstrate that surface heat flux anomalies play a key role in generating the SST pattern seen in Figs. 2b and 6. Anomalies of oceanic heat advection also contribute to the generation of the SST pattern, but with a generally smaller magnitude than the surface heat fluxes. However, oceanic heat advection anomalies are particularly important in regions of large horizontal gradients of temperature such as the Gulf Stream (see Fig. 8).

The above results must be tempered by the caveat that the oceanic heat advection was estimated from monthly mean values, thereby losing variability from timescales shorter than one month. In addition, the conclusions regarding the relative roles of oceanic heat advection versus surface fluxes for this mode of variability may be influenced by the fact that oceanic currents are generally too weak in this model relative to observations. This underestimation of the currents may bias the relative roles of model advective and surface processes relative to the real climate system. However, results from additional model integrations (discussed in the next section) provide very strong

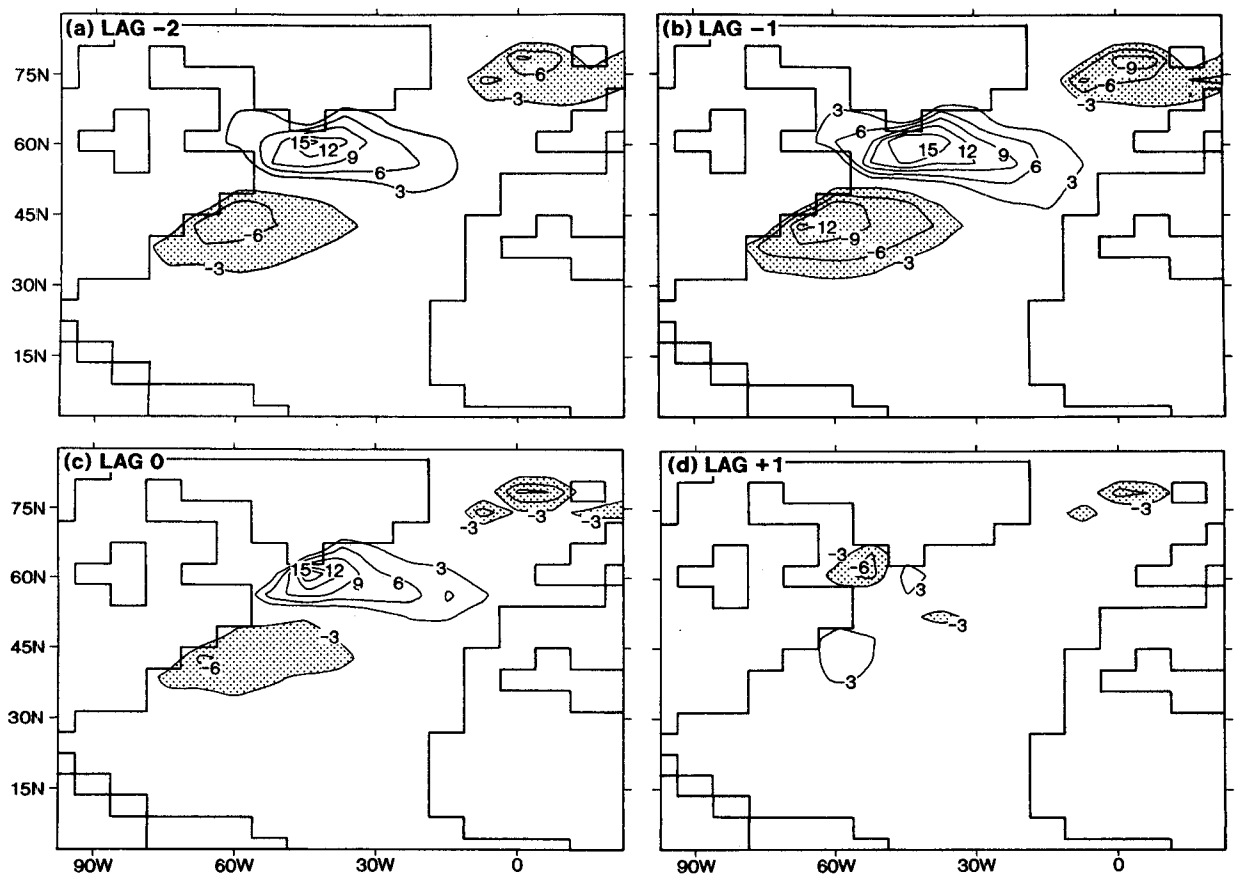

FIG. 9. Same as in Fig. 5 except using the sensible heat flux (W m^{-2}) instead of surface pressure. Contour interval is 3, and values less than −3 are stippled. Positive values indicate an enhanced flux of heat from the ocean to the atmosphere.

corroborating evidence that surface heat flux anomalies are sufficient to drive the mode of oceanic variability seen in Fig. 2b.

As a final note, the flux adjustments [see (2)] play no direct role in this mode of variability. Since the flux adjustments do not vary from one year to the next, there are no monthly anomalies of the flux adjustments and, therefore, no direct impact of the flux adjustment on anomalies of SST.

5. Additional integrations

While the analyses of the above section suggest that the variability seen in Fig. 2b is primarily attributable to atmospheric forcing through the surface heat fluxes, it is desirable to test this hypothesis. Output from additional model integrations will be used to further explore this idea.

Two additional model integrations of length 500 years were analyzed. These additional integrations were designed and conducted by Stouffer et al. (1994) and Manabe and Stouffer (1996) (see these references for further details of the integrations). These additional integrations use the same atmospheric model that was used in the coupled model integration described previously, but they differ from the coupled model in the formulation of the underlying oceanic component of the model. In the first additional integration, a 50-m slab ocean was inserted in place of the fully dynamic ocean in the coupled model. In this experiment (hereafter referred to as the mixed layer experiment), the slab ocean interacts with the atmosphere through the exchange of surface heat and radiative fluxes. In addition, there is a climatological heat flux convergence prescribed at each grid point in order to generate a seasonal cycle of SSTs similar to that in the coupled model. This heat flux convergence mimics the effect of ocean currents on the seasonal cycle of SSTs. Thus, the mean state of the mixed layer model is extremely similar to that of the coupled model. There are no interannual variations of the prescribed heat flux convergence, however. Therefore, oceanic variability present in this model can be attributable only to surface flux or radiative processes—not to ocean dynamics.

In the second additional experiment, SSTs were prescribed from a climatological seasonal cycle and underlie the same atmospheric model used in the coupled

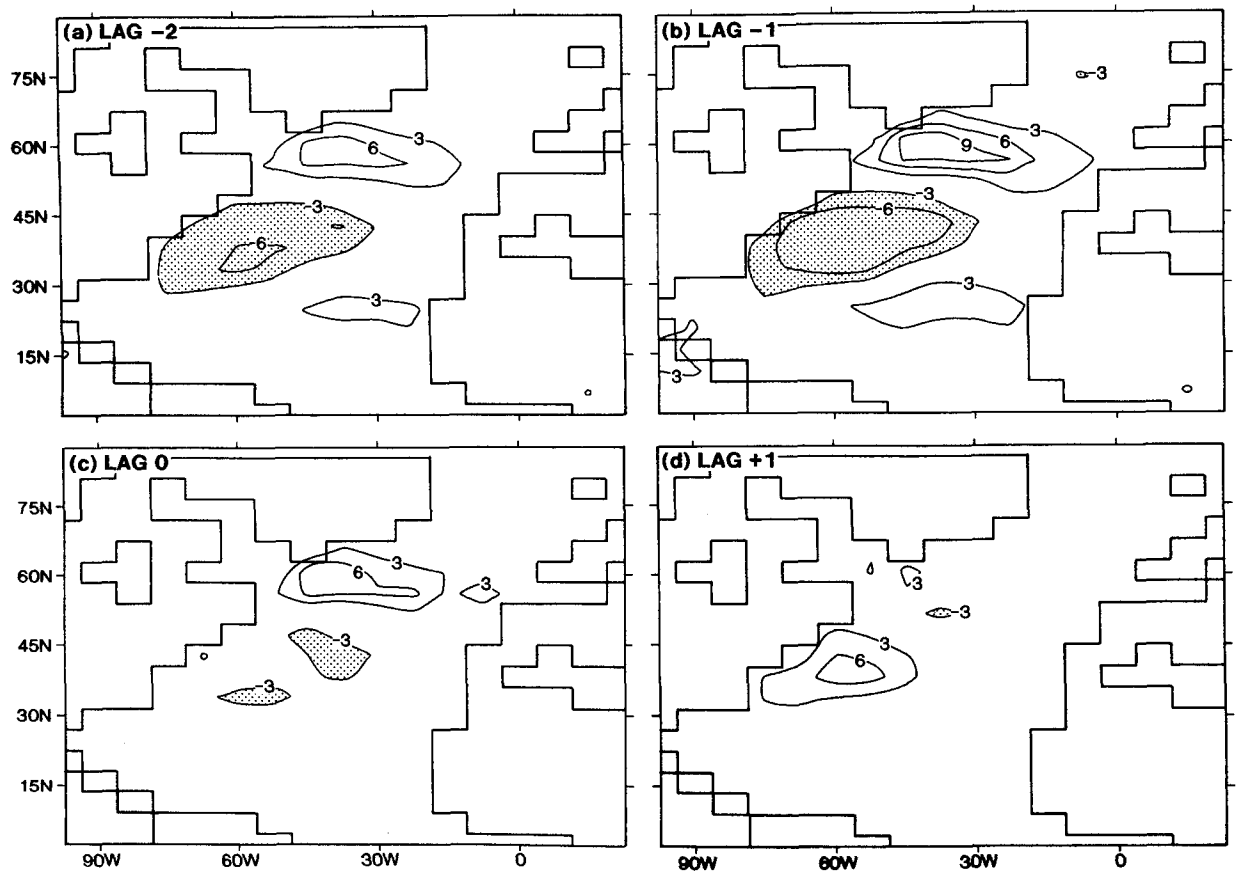

FIG. 10. Same as in Fig. 5 except using the latent heat flux (W m^{-2}) instead of surface pressure. Contour interval is 3, and values less than −3 are stippled. Positive values indicate an enhanced flux of heat from the ocean to the atmosphere.

model. This experiment will be used to examine the primary mode of surface flux anomalies and atmospheric variability in the absence of two way interactions between the atmosphere and ocean (although the ocean still influences the atmosphere in this model). This experiment will be referred to as the prescribed SST experiment.

It is important to note that the mean seasonal and geographical distribution of SST is quite similar for all three experiments. Thus, the model climate fluctuates about similar mean states for each of the model integrations.

Additional diagnostic calculations were also performed using the surface fluxes from the coupled model and the prescribed SST model acting on a 50-m slab ocean.

a. Atmospheric GCM coupled to mixed layer ocean

In order to compare the oceanic variability present in the mixed layer ocean to that from the fully dynamic ocean, an EOF analysis was performed on SSTs averaged over DJF from the mixed layer experiment over the domain 18° to 81°N. The first EOF, explaining 23.0% of the spatially integrated variance, is shown in Fig. 11a. While there are some quantitative differences between this figure and the results from the coupled model (Fig. 2b), the overall pattern resembles the results from the coupled model, suggesting that the surface flux forcing alone is important for generating the mode of SST variability shown in Fig. 2b. Zonally oriented bands of alternating SST characterize the pattern in Fig. 11a, with the maximum in the middle band near the North American coast. The magnitude of the variance explained by this mode in the mixed layer model is, however, substantially larger than that in the coupled model (13%). Since there are no variations of horizontal heat transport in the mixed layer model, it is possible that there are fewer inherent modes of variability in the mixed layer model. Therefore, individual modes that are present explain a higher percentage of the variance.

The primary difference between Figs. 11a and 2b is in the large correlation coefficients near 60°N in the mixed layer results. As discussed in section 4b, oceanic convection and deep vertical mixing play a key role in the heat budget for this region in the model with a dynamic ocean. The presence of such convection and

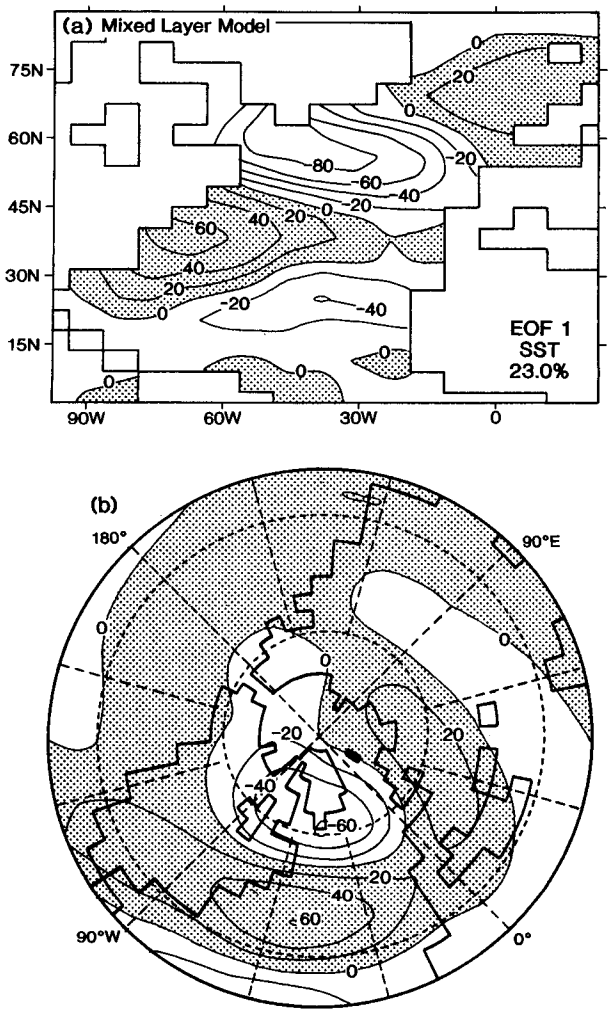

FIG. 11. (a) Spatial pattern of the first EOF of seasonal mean (DJF) SST from the mixed layer model, explaining 23.0% of the spatially integrated variance. The value at each grid point denotes the correlation coefficient (multiplied by 100) between the time series of the first EOF and the time series of model SST at that point. The EOF analysis used the covariance matrix and encompassed a domain extending from approximately 18° to 81°N in the North Atlantic. SST values were multiplied by the square root of the cosine of the latitude in order to weight the grid boxes by their respective area. Values greater than zero are stippled. (b) Linear correlation coefficients (multiplied by 100) between the time series of 500-mb height anomalies at each grid point (DJF averages) and the time series corresponding to the EOF shown in (a). Contour interval is 20.

deep vertical mixing means that the effective mixed layer depth in the coupled model is much deeper at this latitude than the 50-m depth prescribed for the mixed layer experiment. The effective thermal capacity in this region is, therefore, much larger in the coupled model, thus damping the response of the ocean to the surface flux forcing. In contrast, SST anomalies in the mixed layer model are determined solely by the surface heat flux anomalies. This idea is explored below.

In order to quantify the resemblance between Figs. 11a and 2b a pattern correlation coefficient is computed. Specifically, a linear correlation coefficient is computed using pairs of values from corresponding grid points in the two fields over the domain from 18° to 63°N (the region of analysis for Fig. 2b). Using 88 grid points in this domain, the pattern correlation coefficient is 0.74.

The linear correlation coefficients between the time series of the EOF pattern shown in Fig. 11a and the time series of 500-mb height anomalies at each grid point are shown in Fig. 11b. This pattern is similar to that shown in Fig. 2d, suggesting that the same relationship between the modes of atmospheric and oceanic variability that exists in the coupled model is also present in the mixed layer model.

The phase relationship between surface pressure variations and the time series of the EOF of SST was explored in an analogous manner as for the coupled model. The results (not shown) are very similar to Fig. 5, suggesting that atmospheric variability is leading the oceanic variability in the mixed layer model in a similar fashion as in the coupled model. The results for the surface heat flux variations in the mixed layer model (not shown) are very similar to the results from the coupled model. These results suggest that ocean dynamics are not important to this mode of variability.

b. Diagnostic mixed layer

To further test the hypothesis that surface heat flux variations are responsible for the EOF pattern of SST shown in Fig. 2b, we perform an additional series of calculations. Time series of the monthly mean surface heat fluxes from the prescribed SST experiment were used to drive a 50-m slab ocean model. Each grid point consists of a layer of water 50-m thick, whose temperature varies as a result of the prescribed surface fluxes, as well as a damping term. Specifically, the equation governing the slab ocean is

$$\partial T'/\partial t = Q(t)/(\rho d C_p) - \alpha T', \qquad (3)$$

where T' is the deviation of SST from some arbitrary mean, $Q(t)$ is the time series of the prescribed surface heat flux, ρ the density of water ($1\ \mathrm{g\ cm^{-3}}$), d the depth of the mixed layer (50 m), C_p the heat capacity of water ($1\ \mathrm{cal\ g^{-1}\ °C^{-1}}$), and α is the damping coefficient ($1/150\ \mathrm{day^{-1}}$ used here). The damping term (Lau and Nath 1996) is inserted to reflect that in the above formulation the fluxes are not influenced by the temperature of the mixed layer. The magnitude of the damping term is computed from an estimation of what the sensitivity of the surface heat and radiative fluxes would be to the temperature of the mixed layer for constant atmospheric conditions. A number of sensitivity studies were performed which demonstrated that the essential results outlined below are relatively insensitive to the magnitude of this damping term.

Using all 500 years of surface flux data from the prescribed SST model, a 500-year time series of SST is generated. An EOF analysis was performed on this dataset using DJF means, and the first EOF, explaining 21.6% of the variance, is shown in Fig. 12a. There is a resemblance between this pattern and the EOF patterns in Figs. 12a and 2b (the pattern correlation between Figs. 11a and 12a is .97 over the domain from 18° to 63°N; the pattern correlation between Figs. 2b and 12a is .82). This reinforces the notion that variations in the surface fluxes are responsible for this mode of SST variability.

It was speculated above that some of the differences between Figs. 11a and 2b could be attributable to the fact that the mixed layer model had a constant depth of 50 m, whereas the effective mixed layer depth at high latitudes in the coupled model was considerably greater. This idea is tested by repeating the diagnostic calculation, but varying the mixed layer depth as a function of latitude. Specifically, the mixed layer depth is 50 m for all locations south of 45°N and is 500 m for all locations poleward of 60°N. From 45° to 60°N the mixed layer depth increases sinusoidally (from 50 to 500 m). Specifically, where "d" is the depth of the mixed layer and "θ" is latitude,

$$d = 50 + 450^* \sin[(\pi/2)(\theta - 45)/(60 - 45)],$$

$$45 \leq \theta \leq 60.$$

The 500-m depth is arbitrary and is simply meant to illustrate the effect that deeper mixing would have on damping the relative role of surface flux anomalies in forcing SST anomalies. Other values were used and provided similar results. As described above, a 500-year time series of SST was generated, and an EOF analysis was performed. The resulting pattern, shown in Fig. 12b, bears a somewhat better resemblance to Fig. 2b than either Fig. 11a or 12a (the pattern correlation coefficient between Figs. 12b and 2b is .87 over the domain from 18° to 63°N). The greater mixed layer depth at high latitudes effectively dampens the impact of the surface fluxes, thereby producing a smaller signal in SSTs at those latitudes. Therefore, the EOF pattern has its maxima shifted to somewhat lower latitudes where the mixed layer depths are smaller.

The preceding diagnostic calculations were repeated using the time series of the surface fluxes from the coupled model. The spatial patterns of the results described above were essentially unaltered.

c. *Atmospheric GCM with prescribed SSTs*

While the results of the previous section demonstrate that ocean dynamics are not critical to generate the SST pattern shown in Fig. 2b, the possibility remains that the ocean is not simply acting as a slave to the atmosphere but that air–sea interactions play some role. In this context, air–sea "interaction" refers to two way feedback in which the ocean affects the atmosphere and vice versa. This can be explored by examining atmospheric variability in the experiment with a prescribed annual cycle of SST (thereby prohibiting such two-way interactions since there is no feedback from the atmosphere to the ocean). The second EOF of 500-mb height anomalies from this experiment is shown in Fig. 13 (the domain of analysis consists of all points poleward of 20°N; the EOF patterns were rotated using the varimax criterion). This EOF pattern strongly resembles the EOF mode shown from the coupled model in Fig. 3, thereby suggesting that air–sea interactions are not critical for the spatial pattern of this mode of atmospheric variability (although there is still an influence of the ocean on the atmosphere through the surface heat fluxes). It is also interesting that this mode is the second EOF of the prescribed SST experiment. The second and first EOFs of the prescribed experiment resemble the first and second EOFs, respectively, from the coupled experiment.

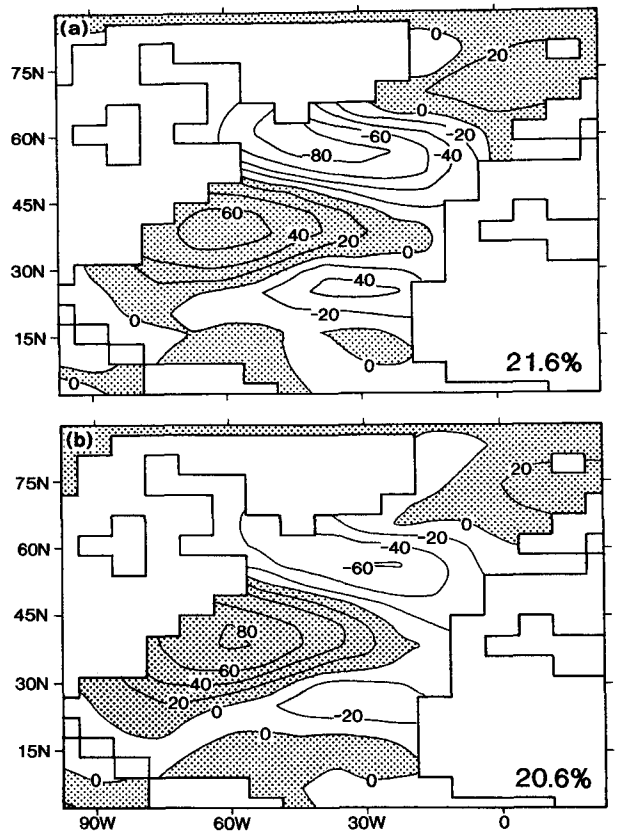

FIG. 12. (a) Same as in Fig. 11a except using SST from the diagnostic mixed layer calculation with uniform mixed layer depth of 50 m. This mode explains 21.6% of the spatially integrated variance. (b) Same as in Fig. 11a except using SST from the diagnostic mixed layer calculation with spatially varying mixed layer depth, as discussed in the text. This mode explains 20.6% of the spatially integrated variance.

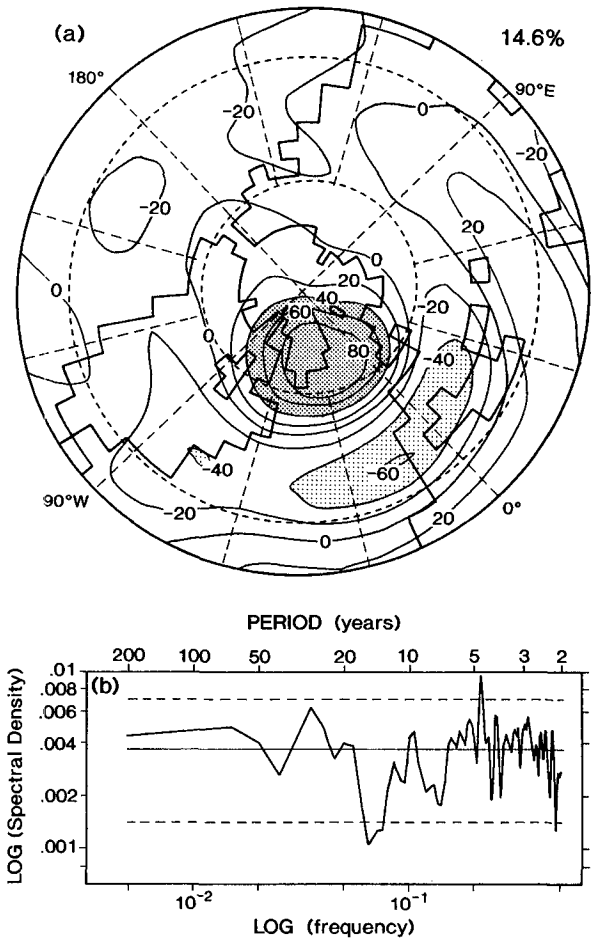

FIG. 13. (a) Spatial pattern of the second EOF of seasonal mean (DJF) 500-mb geopotential height from the experiment with prescribed SST, explaining 14.6% of the spatially integrated variance. The covariance matrix was used, and the domain of analysis consisted of all points poleward of 20°N. (b) Same as in Fig. 4a for the time series corresponding to the EOF shown in (a).

In order to determine whether the variability of the surface fluxes is similar in the prescribed SST experiment to the variability in the coupled model, an EOF analysis was conducted on the surface heat flux anomalies from both experiments. The first EOF of the latent heat flux anomalies from both experiments is shown in Fig. 14. The strong resemblance between the two (pattern correlation = 0.97) suggests that two way air–sea interaction is not critical to the establishment of this mode of variability. Results using the sensible heat flux are similar (not shown; pattern correlation = 0.96 between results from the coupled model and the prescribed SST experiment).

d. Effect of air–sea interactions on atmospheric variability

The preceding analyses suggest that two way air–sea interactions are not critical for establishing the spatial patterns of the atmospheric variability discussed here for this model. This does not imply that such interactions are unimportant for atmospheric variability. Other studies (see, for example, Lau and Nath 1996) have shown that air–sea interactions can have a substantial impact on the variability of the atmosphere by prolonging the timescales of atmospheric fluctuations. In order to briefly examine this issue the standard deviation and month to month persistence of near-surface air temperature were computed using output from the three integrations previously described—the coupled model, the mixed layer model, and the prescribed SST model. The analyses used data from the months of December through February. These results (not shown) confirm that the presence of two way air–sea interactions can increase the persistence of monthly surface air temperature anomalies during winter. The relatively large thermal inertia of the oceanic mixed layer acts as a low-pass filter to the ocean–atmosphere system. The slowly varying mixed layer temperature increases near-surface atmospheric persistence through its effect on

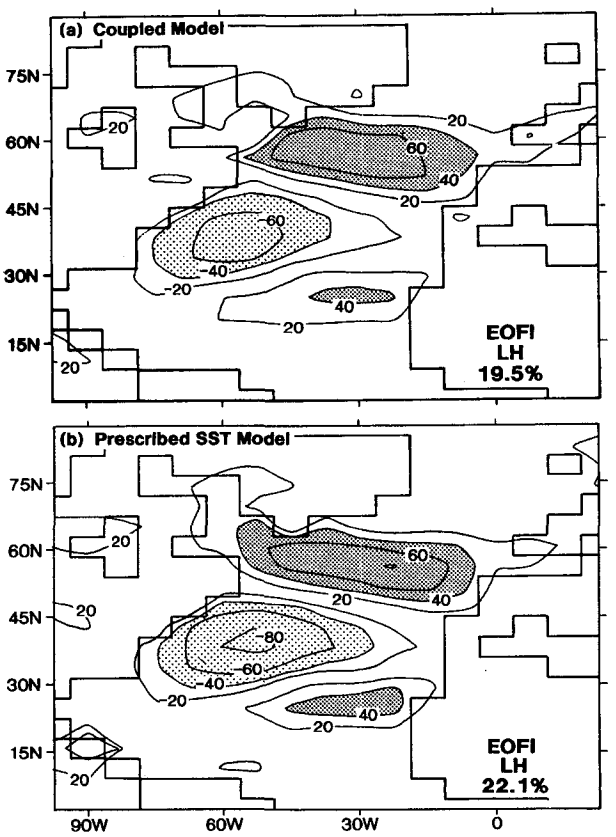

FIG. 14. (a) Spatial pattern of the first EOF of seasonal mean (DJF) latent heat flux from the coupled model experiment, explaining 19.5% of the spatially integrated variance. Domain and technique of analysis as in Fig. 11a. Contour interval is 20. (b) Same as in (a) for the latent heat flux from the prescribed SST experiment. This EOF explains 22.1% of the spatially integrated variance.

the surface heat fluxes. Delworth and Manabe (1993) have shown that an analogous process exists over continental surfaces where the soil layer acts as an integrator of the short time scale precipitation forcing. The slowly varying soil wetness increases the persistence of the near-surface atmosphere through its influence on the surface heat fluxes.

6. Summary and discussion

a. Summary

The primary mode of North Atlantic oceanic variability on interannual timescales has been examined in a coupled ocean–atmosphere model. The model, global in domain with realistic geography and a seasonal cycle of insolation, was integrated for 1000 years. Since previous work (Delworth et al. 1993) had demonstrated that the primary mode of SST variability in the North Atlantic in this model is associated with fluctuations of the thermohaline circulation with a timescale of 40–60 years, the model SST data were filtered such that timescales longer than 30 years were effectively removed. In this manner, analyses could focus primarily on the interannual to decadal timescale.

An EOF analysis of the filtered SST data was conducted using December through February means. The first EOF (shown in Fig. 2b) is characterized by alternating zonal bands of SST anomalies. This pattern bears a distinct resemblance to the observational results (Fig. 2a) from Wallace et al. (1990).

The modes of SST variability in both the observations and model data are related to atmospheric variability in the North Atlantic region. Linear correlations were computed between the time series corresponding to the SST EOF patterns and the time series of 500-mb geopotential height anomalies (shown in Fig. 2c for the observations and Fig. 2d for the model output). This analysis demonstrated that the SST patterns are related to a north–south dipole in 500-mb height, with resemblance to the North Atlantic oscillation and Western Atlantic pattern (see Wallace and Gutzler 1981).

Analyses of the mechanisms responsible for generating the model SST variability demonstrated that the SST variability is primarily forced from atmospheric variability. Fluctuations in the NAO-like pattern of atmospheric circulation in the model create anomalous surface sensible and latent heat fluxes, thereby altering the distribution of SST. The spatial patterns of surface heat flux anomalies in the model resemble observational results (Cayan 1992a). It was found that anomalies of oceanic advection also contributed to this mode of SST variability, but their contribution was generally of a smaller magnitude (at least in this model). Oceanic heat advection anomalies were largest in regions of large horizontal temperature gradient. The conclusions regarding the relative roles of oceanic heat advection versus surface fluxes for this mode of variability should be tempered, however, by the caveat that oceanic currents are generally too weak in this model relative to observations. This underestimation of the currents may bias the relative roles of model advective and surface processes relative to the real climate system.

Results from two additional integrations support the above conclusions. A 500-year integration of the same atmospheric model coupled to a 50-m slab ocean revealed that the first EOF of SST resembles that from the coupled model. In this slab ocean model, SST anomalies can only be generated through surface heat and radiative flux anomalies. This result supports the conclusion that oceanic advection is not critical for this mode of SST variability.

An additional 500-year integration of the same atmospheric model with a prescribed seasonal cycle of SSTs demonstrated that the atmospheric variability present in the coupled model, which is responsible for the SST variability, is also present in the model with prescribed SSTs. Thus, feedbacks from the ocean to the atmosphere do not appear to be critical to the atmospheric variability responsible for the SST variability.

b. Discussion

The present results are in good agreement with recent results of Battisti et al. (1995). In their study, observed perturbations to the surface heat fluxes over the North Atlantic for the period 1950–1988 are used to drive a mixed layer model of the ocean. Their model implicitly includes the climatological effects of heat flux convergence due to ocean currents, but excludes any interannual anomalies of that heat flux convergence. Therefore, this model does not incorporate the impact of oceanic heat advection anomalies on SST variations. This model successfully reproduces observed SST anomalies over the period 1950–1988, thereby supporting the contention that variations in the surface heat fluxes play a crucial role in the generation of interannual variations of SST in the North Atlantic. Namias and Born (1970, 1974) and Alexander and Deser (1995) discussed a mechanism whereby SST anomalies forced from surface heat flux anomalies may persist from one winter to the next.

The spatial patterns of variability of the latent and sensible heat fluxes computed from the model output are in good agreement with the observational results of Cayan (1992a) over the North Atlantic, although the magnitude of model surface flux variations is substantially smaller than observed. In both the observations and the model, surface heat flux variability appears to drive the dominant mode of interannual SST variability.

The results of this study are also in good agreement with the recent work of Lau and Nath (1994) and Graham et al. (1994). In those studies the atmospheric response to SST anomalies over tropical and midlatitude regions was assessed. Both studies concluded that

the response of the atmosphere to midlatitude SST anomalies was much smaller than the response to tropical SST anomalies.

While the results above suggest that the dominant mode of interannual SST variability in the North Atlantic of this model is principally forced by atmospheric variability, the possibility remains that the SST anomaly itself forces an atmospheric response that could contribute to coupled air–sea interactions. Analyses presented here suggest that *for this model* such a response is small. For a more complete discussion of this issue see Kushnir and Held (1996), in which the same atmospheric model as that employed in this paper is forced with idealized SST anomalies in the North Atlantic.

It is critical to stress that the atmospheric response to SST anomalies may be model and resolution dependent. For example, Palmer and Sun (1985), Ferranti et al. (1994), and Peng et al. (1995) describe atmospheric responses in their models to SST anomalies that resemble observational analyses. The existence of such an atmospheric response to an SST anomaly would enhance the possibility of coupled air–sea interactions, rather than the predominantly one-way forcing present in the model employed in this study. For a model with a larger atmospheric response to SST anomalies, the nature and mechanism of seasonal to interannual variability could be substantially different from that suggested by the analyses of this model.

Bjerknes (1964) proposed a paradigm for North Atlantic variability in which SST variations on interannual timescales were principally driven from atmospheric variability, whereas SST variations on the interdecadal timescale were driven more by inherent internal oceanic processes. The results of this paper, combined with the results of Delworth et al. (1993), appear to support this paradigm. Delworth et al. (1993) showed that the dominant mode of variability in the North Atlantic of this model consisted of variations in the thermohaline circulation with a timescale of 40–60 years. Their analyses suggested that the ocean circulation plays a major role in these low-frequency variations of the THC. This may be contrasted with the present results, which show that interannual variations of SST in this model are strongly influenced by surface heat flux variations, which are in turn mainly determined by atmospheric circulation variations. Thus, the two timescales of variability—and the mechanisms responsible for them—that were suggested by Bjerknes (1964) are present in this numerical model. Furthermore, the model variability on the interannual timescale bears a clear resemblance to observational results. On the multidecadal timescale, limited observations hamper our ability to assess the resemblance of the model variability to observations; nevertheless, what limited observational evidence that is available (Kushnir 1994) is encouraging.

One of the motivations for studying Atlantic Ocean variability is the possible role of the ocean in generating atmospheric circulation anomalies, thereby potentially lead to atmospheric predictability. From this point of view, the fact that the atmosphere appears to be forcing the mode of oceanic variability discussed in this paper is discouraging. Since the deterministic limit of atmospheric dynamic predictability is generally thought to be on the order of two weeks, prediction of this mode of SST variability may not be feasible. One hope, however, lies in the extent to which the statistics of the atmospheric flow over the North Atlantic are predictable. For such predictability, the flow would need to be sensitive to slowly varying lower boundary conditions in some other region of the globe, such as the Tropics. In addition, while the surface fluxes appeared to be the primary forcing agent for this mode of model SST variability, other oceanic processes may play a role.

Acknowledgments. The author would like to express his sincere thanks to S. Manabe and R. J. Stouffer, who designed and conducted the three multi-century integrations of the GCM which form the dataset for this paper, and for their encouragement to use their output for the present study. The support of Dr. J. D. Mahlman, GFDL director, is very gratefully acknowledged. Comments on an earlier version of this manuscript by Mike Alexander, Keith Dixon, Steve Griffies, Isaac Held, Yochanan Kushnir, Gabriel Lau, Suki Manabe, Ronald Stouffer, and two anonymous reviewers were extremely useful.

REFERENCES

Alexander, M. A., and C. Deser, 1995: A mechanism for the recurrence of wintertime midlatitude SST anomalies. *J. Phys. Oceanogr.*, **25,** 122–137.

Battisti, D. S., U. S. Bhatt, and M. A. Alexander, 1995: A modeling study of the interannual variability in the wintertime North Atlantic Ocean. *J. Climate,* **8,** 3067–3083.

Bjerknes, J., 1964: Atlantic air–sea interaction. *Advances in Geophysics,* Vol. 10, Academic Press, 1–82.

Bloomfield, P., 1976: *Fourier Analysis of Time Series: An Introduction.* Wiley, 258 pp.

Bottomley, M., C. K. Folland, J. Hsiung, R. E. Newell, and D. E. Parker, 1990: *Global Ocean Surface Temperature Atlas (GOSTA).* Her Majesty's Stationery Office, 20 pp.

Bretherton, C. S., C. Smith, and J. M. Wallace, 1992: An intercomparison of methods for finding coupled patterns in climate data. *J. Climate,* **5,** 541–560.

Bryan, K., 1969: Climate and the ocean circulation: III. The ocean model. *Mon. Wea. Rev.,* **97,** 806–827.

——, and L. J. Lewis, 1979: A water mass model of the world ocean. *J. Geophys. Res.,* **84,** 2503–2517.

Cayan, D., 1992a: Latent and sensible heat flux anomalies over the Northern Oceans: The connection to monthly atmospheric circulation. *J. Climate,* **5,** 354–369.

——, 1992b: Latent and sensible heat flux anomalies over the Northern Oceans: Driving the sea surface temperature. *J. Phys. Oceanogr.,* **22,** 859–881.

Chatfield, C., 1989: *The Analysis of Time Series: An Introduction.* Chapman and Hall, 241 pp.

Daly, A. W., 1978: The response of North Atlantic sea surface temperature to atmospheric forcing processes. *Quart. J. Roy. Meteor. Soc.,* **104,** 363–382.

Delworth, T., and S. Manabe, 1993: Climate variability and land-surface processes. *Adv. Water Resour.*, **16,** 3–20.

——, ——, and R. J. Stouffer, 1993: Interdecadal variations of the thermohaline circulation in a coupled ocean–atmosphere model. *J. Climate,* **6,** 1993–2011.

Deser, C., and M. L. Blackmon, 1993: Surface climate variations over the North Atlantic Ocean during winter: 1900–1989. *J. Climate,* **6,** 1743–1753.

Ferranti, L., F. Molteni, and T. N. Palmer, 1994: Impact of localized tropical and extratropical SST anomalies in ensembles of seasonal GCM integrations. *Quart. J. Roy. Meteor. Soc.,* **120,** 1613–1645.

Frankignoul, C., 1985: Sea surface temperature anomalies, planetary waves, and air–sea feedback in the middle latitudes. *Rev. Geophys.,* **23,** 357–390.

Gordon, C. T., and W. Stern, 1982: A description of the GFDL spectral model. *Mon. Wea. Rev.,* **110,** 625–644.

Graham, N. E., T. P. Barnett, R. Wilde, M. Ponater, and S. Schubert, 1994: On the roles of tropical and midlatitude SSTs in forcing interannual to interdecadal variability in the winter Northern Hemisphere circulation. *J. Climate,* **7,** 1416–1441.

Hasselmann, K., 1976: Stochastic climate models. Part I, Theory. *Tellus,* **28,** 473–485.

Horel, J. D., 1981: A rotated principal component analysis of the interannual variability of the Northern Hemisphere 500-mb height field. *Mon. Wea. Rev.,* **109,** 2080–2092.

Kushnir, Y., 1994: Interdecadal variations in the North Atlantic sea surface temperature and associated atmospheric conditions. *J. Climate,* **7,** 141–157.

——, and I. Held, 1996: Equilibrium atmospheric response to North Atlantic SST anomalies. *J. Climate,* **9,** 1208–1220.

Kutzbach, J. E., 1967: Empirical eigenvectors of sea-level pressure, surface air temperature, and precipitation complexes over North America. *J. Appl. Meteor.,* **6,** 791–802.

Lau, N.-C., and M. J. Nath, 1990: A general circulation model study of the atmospheric response to extratropical SST anomalies observed in 1950–79. *J. Climate,* **3,** 965–989.

——, and ——, 1994: A modeling study of the relative roles of tropical and extratropical SST anomalies in the variability of the global atmosphere–ocean system. *J. Climate,* **7,** 1184–1207.

——, and ——, 1996: The role of the "atmospheric bridge" in linking tropical Pacific ENSO events to extratropical SST anomalies. *J. Climate,* **9,** 2036–2057.

Manabe, S., and R. J. Stouffer, 1988: Two stable equilibria of a coupled ocean–atmosphere model. *J. Climate,* **1,** 841–866.

——, and ——, 1996: Low frequency variability of surface air temperature in a 1000-year integration of a coupled ocean–atmosphere model. *J. Climate,* **9,** 376–393.

——, J. Smagorinsky, and R. F. Strickler, 1965: Simulated climatology of a general circulation model with a hydrological cycle. *Mon. Wea. Rev.,* **93,** 769–798.

——, R. J. Stouffer, M. J. Spelman, and K. Bryan, 1991: Transient response of a coupled ocean–atmosphere model to gradual changes of atmospheric CO2. Part I: Annual mean response. *J. Climate,* **4,** 785–818.

——, M. J. Spelman, and R. J. Stouffer, 1992: Transient response of a coupled ocean–atmosphere model to gradual changes of atmospheric CO2. Part II: Seasonal response. *J. Climate,* **5,** 105–126.

Namias, J., and R. M. Born, 1970: Temporal coherence in North Pacific sea-surface temperature patterns. *J. Geophys. Res.,* **75,** 5952–5955.

——, and ——, 1974: Further studies of temporal coherence in North Pacific sea-surface temperatures. *J. Geophys. Res.,* **79,** 797–798.

Palmer, T. N., and Z. Sun, 1985: A modelling and observational study of the relationship between sea surface temperature in the northwest Atlantic and the atmospheric general circulation. *Quart. J. Roy. Meteor. Soc.,* **111,** 947–975.

Peng, S., L. A. Mysak, H. Ritchie, J. Derome, and B. Dugas, 1995: The differences between early and midwinter atmospheric responses to sea surface temperature anomalies in the northwest Atlantic. *J. Climate,* **8,** 137–157.

Preisendorfer, R. W., 1988: *Principal Component Analysis in Meteorology and Oceanography.* Elsevier, 425 pp.

Stouffer, R. J., S. Manabe, and K. Ya. Vinnikov, 1994: Model assessment of the role of natural variability in recent global warming. *Nature,* **367,** 634–636.

Tziperman, E., and K. Bryan, 1993: Estimating global air–sea fluxes from surface properties and from climatological flux data using an oceanic general circulation model. *J. Geophys. Res.,* **98**(C12), 22 629–22 644.

van Loon, H., and J. C. Rogers, 1978: The seesaw in winter temperatures between Greenland and Northern Europe. Part I: General description. *Mon. Wea. Rev.,* **106,** 296–310.

Walker, G. T., and E. W. Bliss, 1932: World Weather V. *Mem. Roy. Meteor. Soc.,* **4,** 53–84.

Wallace, J. M., and D. S. Gutzler, 1981: Teleconnections in the geopotential height field during the Northern Hemisphere winter. *Mon. Wea. Rev.,* **109,** 784–812.

——, and Q. Jiang, 1987: On the observed structure of the interannual variability of the atmosphere/ocean climate system. *Atmospheric and Oceanic Variability,* H. Cattle, Ed., Roy. Meteor. Soc., 17–43.

——, C. Smith, and Q. Jiang, 1990: Spatial patterns of atmosphere–ocean interactions in the northern winter. *J. Climate,* **3,** 990–998.

Zorita, E., V. Kharin, and H. von Storch, 1992: The atmospheric circulation and sea surface temperature in the North Atlantic area in winter: Their interaction and relevance for Iberian precipitation. *J. Climate,* **5,** 1097–1108.